Biochimica et Biophysica Acta 1861 (2017) 1085–1098

Contents lists available at ScienceDirect

Biochimica et Biophysica Acta

journal homepage: www.elsevier.com/locate/bbagen

Inactivation of iron-sulfur cluster biogenesis regulator SufR in *Synechocystis* sp. PCC 6803 induces unique iron-dependent protein-level responses

Linda Vuorijoki, Arjun Tiwari, Pauli Kallio, Eva-Mari Aro *

Molecular Plant Biology, Department of Biochemistry, University of Turku, FI-20014 Turku, Finland

ARTICLE INFO

Article history:
Received 18 November 2016
Received in revised form 31 January 2017
Accepted 14 February 2017
Available online 16 February 2017

Keywords:
Synechocystis sp. PCC 6803
Iron-sulfur clusters
Gene regulation
SRM proteomics
EPR spectroscopy
RT-qPCR

ABSTRACT

Background: Iron-sulfur (Fe-S) clusters are protein-bound cofactors associated with cellular electron transport and redox sensing, with multiple specific functions in oxygen-evolving photosynthetic cyanobacteria. The aim here was to elucidate protein-level effects of the transcriptional repressor SufR involved in the regulation of Fe-S cluster biogenesis in the cyanobacterium *Synechocystis* sp. PCC 6803.
Methods: The approach was to quantitate 94 pre-selected target proteins associated with various metabolic functions using SRM in *Synechocystis*. The evaluation was conducted in response to *sufR* deletion under different iron conditions, and complemented with EPR analysis on the functionality of the photosystems I and II as well as with RT-qPCR to verify the effects of SufR also on transcript level.
Results: The results on both protein and transcript levels show that SufR acts not only as a repressor of the *suf* operon when iron is available but also has other direct and indirect functions in the cell, including maintenance of the expression of pyruvate:ferredoxin oxidoreductase NifJ and other Fe-S cluster proteins under iron sufficient conditions. Furthermore, the results imply that in the absence of iron the *suf* operon is repressed by some additional regulatory mechanism independent of SufR.
Conclusions: The study demonstrates that Fe-S cluster metabolism in *Synechocystis* is stringently regulated, and has complex interactions with multiple primary functions in the cell, including photosynthesis and central carbon metabolism.
General significance: The study provides new insight into the regulation of Fe-S cluster biogenesis via *suf* operon, and the associated wide-ranging protein-level changes in photosynthetic cyanobacteria.

1. Introduction

Iron-sulfur (Fe-S) clusters are a group of essential cofactors involved in a number of metabolic processes, such as photosynthesis, respiration and nitrogen fixation [1]. The biologically relevant redox range of the clusters, from −710 mV of the F_X cluster in photosystem I [2] up to approximately +280 mV of Rieske Fe-S cluster in cytochrome b_6f [3–5], enables the Fe-S clusters to be utilized in catalytic redox reactions and in redox sensing as part of gene regulation [6]. In environments which induce oxidative stress, such as iron limiting conditions [7], the Fe-S cluster integrity and function are compromised due to their oxygen sensitivity [8], which readily leads to destabilization and degradation of the clusters with consequent inactivation of the corresponding proteins.

In oxygen-producing cyanobacteria, the Fe-S clusters are constantly exposed to oxygen and more importantly, to semi-reduced oxygen radicals that are generated in photosynthetic light reactions. Destabilization of Fe-S clusters by oxygen radicals and the subsequent release of catalytic Fe^{2+}-iron provoke inactivation of various Fe-S proteins [9]. Damaged Fe-S clusters, in turn, limit photosynthetic electron transfer especially in photosystem I (PSI), which harbours altogether three electron-transferring [4Fe-4S] clusters; F_X ligated to the PsaA and PsaB subunits and the F_A and F_B clusters in the PsaC subunit of PSI [10,11]. Damage in PSI escalates the oxidative stress as it causes the over-reduction of the photosynthetic electron transport chain, which consequently generates more reactive oxygen species (ROS).

Sufficient availability of iron is crucial for the maintenance of various metabolic processes requiring iron cofactors such as heme, non-heme or Fe-S clusters. Iron is especially important for the photosynthetic machinery, where as many as 12 Fe molecules are associated with PSI, and

Abbreviations: Fe-S cluster, iron-sulfur cluster; ROS, reactive oxygen species; PSI/II, photosystem I/II; SUF, sulfur utilization factor; SRM, selected reaction monitoring; EPR, electron paramagnetic resonance; RT-qPCR, real time quantitative polymerase chain reaction; HPLC, high performance liquid chromatography; IAA, iodoacetamide; DTT, dithiotreitol; FeCN, potassium ferricyanide.

* Corresponding author at: Molecular Plant Biology, BioCity A, Tykistökatu 6 A, 6th floor, Department of Biochemistry, University of Turku, 20014 Turku, Finland.
E-mail addresses: lkvuor@utu.fi (L. Vuorijoki), arjtiw@utu.fi (A. Tiwari), pataka@utu.fi (P. Kallio), evaaro@utu.fi (E.-M. Aro).

http://dx.doi.org/10.1016/j.bbagen.2017.02.020

additionally PSII, cytochrome b_6f and cytochrome c-553 harbor altogether ten molecules of iron [12–15]. The relatively high requirement for iron, which is at least one order of magnitude higher iron quota than in non-photosynthetic bacteria [16–18], often causes cyanobacteria to encounter iron deficiency in the natural environment. Iron limitation easily results in an amplified effect, where the decrease in iron-containing enzymes which fight against oxidative stress [7,19] leads to increased oxidative stress and further damage to the Fe-S clusters. Consequently, oxidative stress induces the Fenton reaction, where the Fe^{2+} released from the degraded Fe-S clusters reacts with hydrogen peroxide (H_2O_2), causing oxidization and precipitation of iron as ferric hydroxides while hydroxide (OH^-) and hydroxyl radicals ($OH^{\bullet}$) are formed. Thus, the iron depletion feeds itself and gets more pronounced, resulting in extensive changes in the electron transport network.

To cope with the limited amounts of iron in the oceanic and fresh water environments, cyanobacteria have developed several iron transport and storage mechanisms. Iron can be acquired from the scarce extracellular pool of iron, which exists as free, inorganic form or as complexes with siderophores, which are secreted by some cyanobacterial species. The free or chelated iron is transported to the cell through the outer membrane via TonB-ExbB-ExbD system [20] and then internalized through plasma membrane either as ferrous or ferric form. The reductive iron uptake through the Fe^{2+} specific FeoB transporter has been shown to be the most effective transport system, while the Fe^{3+} specific FutABC complex works as a complementary transporter system [21]. Once inside the cell, the ferrous iron is typically sequestered by the ferritin family proteins and stored as ferric iron [18]. Upon iron depletion, the stored iron is mobilized by the induction of yet another type of ferritin protein, MrgA, in order to alleviate the need for externally obtained iron [18]. At the same time, besides the increased expression of iron transporters which enhance iron uptake, there is an increase in proteins which can substitute for the iron-containing proteins. These include the *i*ron *s*tress *i*nducible flavodoxin (IsiB), which replaces the Fe-S-containing ferredoxin as electron carrier protein [22]. Flavodoxin is co-expressed with the chlorophyll binding IsiA (CP43′) protein, which functions as an extra antenna for PSI under iron deficiency but also enhances the thermal dissipation and protection of the cells from photo-oxidative stress under iron deprivation [23–26]. The iron deficiency also strengthens the preference of plastocyanin instead of heme-bearing cytochrome c553, as an electron carrier between cyt b_6f and PSI [27,28].

In order to maintain a balance between available iron and the processes which depend on it, Fe-S cluster biogenesis and the regulation of the associated enzymes are directly linked with the overall iron metabolism network of the cell. Transcription factors that regulate gene expression in response to the redox state of the bound Fe-S clusters, function as sensors of the available iron and cellular redox poise [29]. One of these transcriptional factors is SufR (*sll0088* in *Synechocystis* sp. PCC 6803; *Synechocystis* from hereon), a homodimeric protein which binds one [4Fe-4S]-cluster per subunit and acts as a repressor of the *sufBCDS* operon [30,31]. The operon is part of the SUF-system, which contributes to the Fe-S cluster biogenesis in cyanobacteria as well as in many non-photosynthetic bacteria [30–33]. The components of the SUF system have been extensively studied mainly in *Escherichia coli* [32,33], and the SufB, SufC and SufD have been shown to interact with each other and to form an Fe-S cluster assembly complex. This complex interacts with the SufSE complex, which is responsible of the transfer of sulfide into the cluster [32,34]. The SufBCD itself is suggested to participate in iron mobilization and transfer of Fe-S-cluster to the target proteins. The energy required for this is most probably acquired from SufC, which is an unorthodox ABC/ATPase [35]. The function of the Suf proteins in cyanobacteria has not been thoroughly elucidated, but based on the current knowledge it is expected to resemble the corresponding system in non-photosynthetic bacteria.

Oxidative stress, which inflicts damage to the SufR Fe-S clusters, reduces the binding affinity of SufR to the *sufBCDS*-promoter region, which leads to derepression of the *suf* operon [30,31]. Accordingly, chromosomal inactivation of *sufR* has been shown to result in increased transcript levels of *suf* operon genes in *Synechococcus* sp. PCC 7002 (hereafter *Synechococcus*) both under iron sufficient and deprived growth conditions [30]. A similar response, although more pronounced, is observed under iron limiting conditions in the wild type (WT) strain. Based on the highly conserved sequence around the *sufR-sufBCDS* region, the overall mechanism is expected to be similar also for *Synechocystis* [30].

This study focused on the elucidation of the role of SufR, the transcriptional repressor of the *suf* operon, under iron sufficient and deprived conditions in *Synechocystis*. The strategy was to subject 94 preselected target proteins, either directly associated with Fe-S cluster metabolism or having specific key functions in the cell, for quantitative proteomics analysis upon inactivation of the SufR protein. To assess the correlation between the amount and functionality of addressed Fe-S proteins, the protein quantification was further evaluated against the functional status of the Fe-S proteins and protein complexes involved in photosynthesis as well as with respect to changes on transcript levels.

2. Materials and methods

2.1. Strains and growth conditions

The cyanobacterial strains used in this study were the *Synechocystis* sp. PCC 6803 WT and the generated Δ*sufR* strain. The strains were cultivated under photoautotrophic conditions in AlgaeTron AG 230 growth chamber (Photon Systems Instruments, Drásov, Czech Republic), under controlled, 1% (vol/vol) CO_2 conditions. The temperature was set to +30 °C and the light intensity to 50 μmol photons m^{-2} s^{-1}. The cells were grown in BG-11 medium [36], buffered with 20 mM TES-KOH (pH 8.0) in Erlenmeyer culture flasks on a rotary shaker (120 rpm). The precultures (40 ml BG-11 in 100 ml flasks) were grown under standard BG-11 media until mid-logarithmic phase, harvested by centrifugation and washed either once or three times with standard or iron depleted (no added $FeNH_4$-citrate) BG-11 media, respectively. The precultures were used to inoculate the main cultures (40 ml BG-11 in 100 ml flasks) to the starting $OD_{750\ nm}$ of 0.1. The cell density was estimated by measuring the optical density at 750 nm ($OD_{750\ nm}$) with a Genesys 10S UV–VIS spectrophotometer (Thermo Scientific). The Δ*sufR Synechocystis* cells for SRM analyses were harvested from both iron sufficient (+Fe) and deprived conditions (−Fe) at $OD_{750\ nm}$ 1.0 (short-term treatment), at approximately 62 h (+Fe) and 81 h (−Fe), and at 12 days under iron deprivation (long-term treatment). The corresponding WT samples used for comparison were collected and analyzed at 57 h (+Fe), 76 h (−Fe) and after 12 days [37].

2.2. Construction of sll0088 deletion mutant

In order to inactivate SufR in *Synechocystis*, a deletion construct was designed to disrupt the native *sufR* gene (*sll0088*) by insertion of a chloramphenicol resistance cassette (Cm^R) by homologous recombination. The deletion construct was assembled by fusion PCR [38], using WT *Synechocystis* chromosomal DNA and pACYCDuet-1 (Novagen) as the PCR templates for the homologous regions and Cm^R, respectively. The chromosomal DNA was isolated by phenol-chloroform extraction from *Synechocystis* WT; the colonies were inoculated to 1× TE-buffer (10 mM Tris-HCl/0.1 mM EDTA), heated at +65 °C for 10 min in equivalent volume of saturated phenol (Sigma-Aldrich) and centrifuged (5 min; 10,000 ×*g*), after which the supernatant was washed twice with chloroform (Sigma-Aldrich). The PCR primers (Oligomer) used for generating the construct are listed in Table 1. Primers P1(fw) + P2(rev) and P3(fw) + P4(rev) were used for the amplification of the 5′ (269 bp) and 3′ regions (245 bp) of *sll0088*, respectively, whereas complementary primers P5(fw) + P6(rev) allowed the amplification of the Cm^R (1228 bp). The three PCR products were isolated from 1% agarose gel, extracted (QIAEX® II Gel Extraction Kit) and used as templates to compile the final deletion construct using the primers P7(fw) + P8(rev).

Table 1
Sequences of the PCR primers used for constructing and verification of the *sufR* deletion mutant.

Primer name	Sequence 5′ to 3′
P1(fw)	TTGTCCTTTCAGTTTACTGGACTGC
P2(rev)	GGTGTTTTTGAGGTGCTCCAGTGGATAGAGAAATTGGGGTCTGCCC
P3(fw)	GCTAGTTATTGCTCAGCGGTGGCATACGGCGGCAGGAAGGTTATATG
P4(rev)	TTAGTTCGGGGTTTTAGACTGG
P5(fw)	CCACTGGAGCACCTCAAAAACACC
P6(rev)	TGCCACCGCTGAGCAATAACTAGC
P7(fw)	TCTCCTGTTGTTGACCATGACC
P8(rev)	AGGTGTGTTCCCCATCATTAAGCC
P9(fw)	GCATCTACCGCCACATTACTTAAACG
P10(rev)	CCTCAACGGCTACGATGTCTTGCAGG

2.3. Transformation of sufR deletion construct to Synechocystis

WT *Synechocystis* was transformed by adding approximately 1 μg of purified *sufR* deletion construct to 100 μl of concentrated cell culture. The DNA-cell mixture was incubated in a shaker o/n at + 30 °C in darkness and plated on BG-11. After 48 h, chloramphenicol was supplemented to the transformant plate to a final concentration of 10 μg/ml.

To obtain a segregated *Synechocystis* Δ*sufR* mutant line, the transformant colonies were restreaked multiple times under chloramphenicol selective pressure. The complete segregation of the mutant was verified by colony PCR analyses, which were carried out with primers P9(fw) and P10(rev) (Table 1) amplifying either 2 kb (WT) or 3 kb (Δ*sufR*) fragments of the *Synechocystis* genome.

2.4. In vivo absorption spectra

In vivo absorption spectra were measured with an Infinite 200 PRO multiplate reader (Tecan) from 400 to 750 nm to follow the induction of iron deprivation in the Δ*sufR* mutant and WT cells by the characteristic shift in chlorophyll *a* (chl *a*) absorbance as well as changes in other pigments such as phycobilisomes (at approx. 626 nm) and carotenoids (at approx. 480 nm).

2.5. Protein quantification by SRM

The SRM-experiments followed the workflow described by Vuorijoki et al. [37]. The proteins were extracted as whole cell lysate in 0.1 M ammonium bicarbonate (NH_4HCO_3) buffer containing 8 M urea, 0.1% (w/v) Rapigest SF (Waters Corporation, Milford, MA) and 0.2 mM PMSF protease inhibitor. An equal volume of acid washed glass beads (150–212 μm, Sigma) was added to the solution and the cells were disrupted with bead beater (Mini-Bead-Beater-8, Unigenetics Instruments Pvt. Ltd., India). The protein concentration was determined from the supernatant with the Bradford assay [39]. Proteins were reduced by dithiotreitol (DTT; Sigma) and alkylated with iodoacetamide (IAA; Sigma), at final concentrations of 5 mM and 10 mM, respectively, followed by acetone/ethanol precipitation at −20 °C. The protein pellets were digested o/n in 50 mM NH_4HCO_3 and 5% (v/v) acetonitrile buffer with two additions of trypsin (Sequence grade Modified, Promega, Madison, WI, USA) with 1:100 (w/w) trypsin to protein ratio. The peptides were then desalted with Solid Phase Extraction technique and biological triplicates were loaded as 150 ng/5 μl injection to nanoflow HPLC system (EasyNanoLC 1000; Thermo Fisher Scientific). The peptides were separated by using a 60 min non-linear gradient at a flow rate of 300 nl/min (5–20% B in 35 min; 20–35% B in 50 min; B = acetonitrile:water, 98:5). Thereafter, the peptides were ionized by a nano-electrospray and analyzed in triple quadrupole mass spectrometer (TSQ Vantage, Thermo Scientific). The mass spectrometer operated in SRM mode with the settings described in [37]. The precursor to fragment ion transitions were measured with 2.5 s cycle time with minimum 20 ms dwell time for each transition.

The SRM data-analysis including the peak picking and identification was done in Skyline [40] and the relative quantification was performed with MSstats (3.1.4) package [41,42]. A global standard normalization was used with two endogenous peptides (SNLDSNHIIYR and SEELLGAASNR) of the probable DNA-directed RNA polymerase omega subunit (*ssl2982*).

Altogether 94 proteins with validated SRM-assays [37] were targeted in this study in *Synechocystis* Δ*sufR* mutant cultured under different iron conditions, and compared with previously published data in the WT strain. The SRM-assay information could be retrieved from Panorama Public (https://panoramaweb.org/labkey/Vuorijoki_et_al_2015.url) and PASSEL with PASS00726 identifier (http://www.peptideatlas.org/PASS/PASS00726). For the quantification of six proteins (encoded by *sll0542*, *sll1031*, *sll1525*, *slr1963*, *slr2067*, *slr2136*), a different set of 2–3 proteotypic peptides were selected, due to more stable signals between the replicates. These peptides (*sll0542;* SLASGQEISGDTSTLEDR, *sll1031*; SAVAHQTGNLAGDSANQLR, *sll1525*; GHTYEDILASINAR, *slr1963*; GVTEPAEDGFTQIK, *slr2067*; SIVNADAEAR, *slr2136*; EGYSDQEFAEIGEK) can be found in the MSstats input file (Table 2 in [43]) as well as in the datasets deposited in Panorama Public and PASSEL with the assay parameters (accession information in Results section). The indexed retention times (iRT-values) for these peptides can be found in Table 1 of [43].

2.6. Quantification of functional PSII and PSI complexes by EPR

The electron paramagnetic resonance (EPR) spectroscopy was performed with intact *Synechocystis* cells at room temperature to quantify the relative amounts of PSII and PSI. The cells grown in standard BG-11 medium (+Fe) were harvested at $OD_{750\ nm} = 1$ and the iron starved cells grown in iron depleted BG-11 medium (−Fe) were harvested after 12 days. The chl *a* concentration was determined prior harvesting and used to adjust the final chl *a* concentration in the samples to 4 mg/ml. Chlorophyll was extracted with 90% methanol and the absorbance at 665 nm was multiplied with an extinction coefficient of 78.74 $l\ g^{-1}\ cm^{-1}$ to determine the chl *a* concentration [44]. The EPR measurements were performed with Miniscope (MS5000) EPR-spectrometer, equipped with variable temperature controller (TC-HO4) and Hamamatsu light source (LC8). The measurements were conducted with the frequency of 9.44 GHz, center field of 336.5 mT, microwave power of 3 mW, field sweep of 9 mT and modulation frequency of 100 kHz with modulation width of 0.5 mT. In order to fully oxidize tyrosine $D^{\bullet}$ (representing the amount of functional PSII), the samples were first illuminated with continuous saturating light (5000 μmol photons $m^{-2}\ s^{-1}$) for 150 s. Prior the measurements, samples were dark-adapted for 1 min to obtain a stable and fully oxidized tyrosine $D^{\bullet}$ radical as described by Tiwari et al. [45]. In order to ensure the full oxidation of $P700^{+}$ (representing the amount of functional PSI), two different methods were tested. First one included photo-oxidation of P700 in the presence of DCMU (10 μM), which blocks the electron transfer to PSI, causing accumulation of $P700^{+}$ and Tyr $D^{\bullet}$ during continuous illumination [46]. To calculate the quantity of oxidized $P700^{+}$ from the DCMU treatment, the Tyr $D^{\bullet}$ signal obtained as post-illuminated dark spectrum was subtracted from the spectrum measured during continuous illumination [46]. The other tested method was based on chemical oxidation in dark using 100 mM of PSI electron acceptor potassium ferricyanide, $K_3[Fe(CN)_6]$ (from hereon FeCN), which specifically generates only $P700^{+}$ signal. As the quantity of oxidized PSI was nearly the same after both treatments (Appendix Fig. A.1), the chemical oxidation by FeCN was preferred in the subsequent analysis for $P700^{+}$ oxidation. The relative quantification of $P700^{+}$ was performed by dividing the spin numbers of $P700^{+}$ with that of tyrosine $D^{\bullet}$ on equal chlorophyll basis.

2.7. RNA isolation, cDNA synthesis and RT-qPCR

30–40 ml of cells cultured under the different test conditions were harvested by centrifugation at 5000 rpm for 6 min at 4 °C (TX-400

rotor, SL 16R centrifuge, Thermo Scientific), followed by immediate freezing of the pellets by dipping the tubes in liquid N_2. The cells were then thawed on ice, washed with cold resuspension buffer containing 0.3 M sucrose and 10 mM sodium acetate (as described in [47]), and re-frozen as before for storage at −80 °C. For RNA isolation, the pellets were thawed on ice and suspended in 200 μl resuspension buffer, followed by addition of lysis buffer to obtain the final concentrations of 25 mM EDTA (pH 8.0), 1% SDS and 10 mM sodium acetate (adapted from [48]). To isolate the RNA, the samples were extracted multiple times with 1:1 volume of hot acidic phenol:chloroform (1:1) until the aqueous phase (top phase containing the RNA) was free of protein impurities (white precipitate at the solvent interphase). Remaining phenol in the aqueous sample was removed by an additional extraction with an equal volume of chloroform. RNA was precipitated by incubating the sample o/n at −20 °C in the presence of 0.56 M LiCl and 67% ethanol. The co-precipitated genomic DNA was removed by 30 min DNase (2 U) (TURBO DNA-free kit, Ambion) treatment according to manufacturer's instructions. RNA concentration was measured with BioDrop μLITE (BioDrop Ltd.) and the RNA integrity was verified on 1.2% agarose gel. Complementary DNA (cDNA) was synthesized from 1 μg of DNA free RNA using iScript™ cDNA synthesis kit (BioRad). The cDNA was diluted five-fold and 5 μl of each triplicate sample of both WT and Δ*sufR* strain was used as a template for RT-qPCR.

The RT-qPCR was performed on iCycler IQ Thermal Cycler (v. 4.006) and the data was analyzed by iQ™5 Optical System Software (v. 2.0) (Bio-Rad), using iQ SYBR Green Supermix (BioRad). The optimal annealing temperature for each amplicon (Table 2) was tested on a gradient PCR run from 53.8 °C to 62.5 °C, and the PCR protocols were designed accordingly (3 min initial denaturation at 95 °C followed by 40 cycles of 95 °C for 10 s, 57 °C or 59 °C for 30 s and 72 °C for 20 s). Melting curve analysis was performed as described in [47]. The efficiencies of amplicon groups were calculated from a standard curve where a five-fold dilution series of cDNA was plotted against threshold cycles (C_T-value) of each dilution. The changes in gene expression relative to the WT were calculated by Pfaffl method, taking into consideration the different amplification efficiencies (E) of each amplicon (Table 2) [49]. The *rimM* (*slr0808*, encoding 16S rRNA processing protein) was used as a normalization gene for the calculations [47]. Samples which were not treated with reverse transcriptase served as negative controls.

3. Results

3.1. Inactivation of sufR in Synechocystis sp. PCC 6803

The *sufR* gene (*sll0088*), encoding the *suf* operon repressor protein SufR in *Synechocystis*, was inactivated using homologous recombination by targeted insertion of a chloramphenicol resistance (Cm^R) cassette

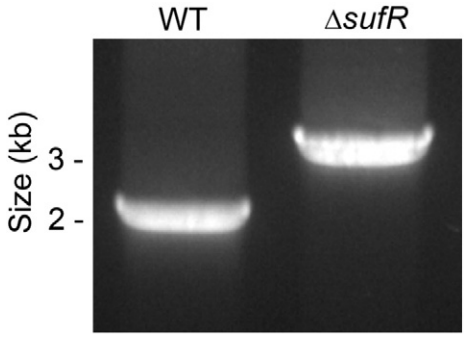

Fig. 1. Agarose gel electrophoresis showing the *sufR* colony PCR products of WT *Synechocystis* (2 kb) and Δ*sufR* mutant strain (3 kb).

201 bp downstream from the second start codon [31]. This resulted in the replacement of a 202 bp fragment in the middle of *sufR* with a 1228 bp insert, separating the N-terminal DNA-binding motif from the C-terminal domain associated with [4Fe-4S] cluster binding [30,31]. The chloramphenicol resistant transformant colonies were screened using colony PCR in order to confirm the integration in the *sufR* locus. The colonies were streaked for several generations under antibiotic selection pressure to obtain complete segregation of the mutation. In the final screening, only amplification fragments corresponding to the disrupted Δ*sufR* (~3 kb) were observed while the WT *sufR* fragments (~2 kb) could not be detected (Fig. 1).

Despite the segregated *sufR* deletion, SufR-derived peptides were detected in the subsequent SRM analysis in the mutant samples. The signals originated from the truncated inactive polypeptide (68 amino acids) expressed from the 5′ end of disrupted Δ*sufR*, upstream of the inserted chloramphenicol cassette, which still harbored the native regulatory sequences; the only suitable SRM-peptides (proteotypic peptides; PTPs) applicable for SufR quantification in the assay (Appendix Fig. A.2) were located in this region. However, the signal intensities remained marginal due to mRNA instability or rapid turnover of the misfolded protein fragments, and unlike in the WT strain, the SufR SRM-signals of the Δ*sufR* mutant did not increase in response to the induced expression of SufR under iron depletion (Table 3, Fig. 2). In addition, the inactivation of SufR was demonstrated by the release of the repression of *suf* operon expression under iron sufficient conditions in the subsequent analysis of the Δ*sufR* mutant strain (Fig. 3).

3.2. Phenotype of the ΔsufR mutant

The Δ*sufR* mutant strain could not be distinguished from the WT *Synechocystis* based on growth rate either under iron sufficient or

Table 2
Primers used in RT-qPCR and the optimal annealing temperature and amplification efficiency (E) for each amplicon. Asterisk (*) refers to unspecific primer dimer signals, which affect the amplification efficiency and give signals at late amplification cycles.

Primer name	Primer sequence 5′→3′	Optimal annealing temperature (°C)	Amplification efficiency, E
sufR/sll0088_fw	AAACAGTGGGGGAAGAACAGT	57	3.47*
sufR/sll0088_rev	CCGTAGCTCCACCAGTTTATGT		
fed2/sll1382_fw	ACAGCGTGATTGTCTCCGAC	57	2.02
fed2/sll1382_rev	TTGCCCAGAAATAACCCGCA		
sdhB/sll0823_fw	TTGCCGTAATGCCATCTGTG	57	2.07
sdhB/sll0823_rev	ACTGATGGTGAAAACTCCGGT		
sufB/slr0074_fw	CCATGGAATTGTCCACCTATTT	59	2.11
sufB/slr0074_rev	GCATGAAGTTGATTGGTGTCAT		
fed4/slr0150_fw	TTTGCCCTATTCCTGTCGGG	59	2.02
fed4/slr0150_rev	CACAGAGCAACACACAACCC		
synifU/ssl2667_fw	AACTCCGTCCCTACCTGATG	59	2.01
synifU/ssl2667_rev	TAGGGTCATGGTGGAACTGG		
nifJ/sll0741_fw	GGCCTACCTGCTCAGTGAAG	59	1.87
nifJ/sllO741_rev	CCTCGCTTTGCATTTCCACC		
rimM/slr0808_fw	GGGAATTCCACGTCACTGAT	57/59	1.86
rimM/slr0808_rev	GGGACGAGCACTTCTTTGTC		

Table 3
The expression level fold changes of targeted proteins in WT and Δ*sufR* under all experimental conditions (I to III are short-term experiments, IV and V are long-term experiments) in comparison to WT under iron sufficient conditions. The values are in $\log_2$ scale. The small font sizes indicate measurements with adjusted p-values > 0.01. The red and green gradients represent the amplitude of upregulation and downregulation of the proteins, respectively. The asterisk (*) indicates that the respective protein binds either Fe or Fe-S-binding motifs based on UniProt and Cyanobase annotations and literature.

Gene	Protein symbol	I. ΔsufR +Fe	II. WT −Fe	III. ΔsufR −Fe	IV. WT −Fe (12d)	V. ΔsufR −Fe (12d)	Metabolic context / function	Functional category
sll1831	GlcF*	0.32	−2.96	−1.65	−1.15	−0.55	Glycolate pathway	Catabolism/ amphibolic pathways
sll1196	PfkA	−0.01	0.32	0.54	0.59	0.53	Glycolysis	
slr1843	Zwf	−0.32	0.99	1.15	1.86	1.85	Pentose phosphate pathway	
sll0741	NifJ. Pfo*	−1.20	−3.73	−4.08	−2.83	−2.69	Pyruvate and acetyl–CoA metabolism	
sll0542	Acs	−0.59	−0.18	−0.28	0.26	0.01		
sll0920	Ppc	−0.20	0.94	0.95	1.95	1.69		
slr0665	AcnB*	−0.64	−1.92	−1.74	−0.53	−0.68	TCA cycle	
slr1289	Icd	−0.19	0.70	0.66	1.53	1.52		
sll0823	SdhB*	−1.12	−2.14	−1.96	−1.64	−1.68		
sll1625	SdhB*	−0.53	−1.49	−1.36	−0.54	−0.38		
sll0158	GlgB	−0.33	0.96	1.07	1.46	1.44	Carbohydrate metabolism	Other anabolic reactions/ auxiliary metabolism
sll1356	GlgP*	−0.09	0.52	0.64	1.49	1.33		
sll0169	ZipN. Ftn2	−0.04	0.45	0.51	1.34	0.93	Cell division	
slr0417	GyrA	−0.44	0.76	0.90	1.02	0.86	DNA unwinding	
sll0698	DspA/Hik33	−0.25	0.34	0.38	0.37	0.32	Drug and analog sensitivity	
sll0728	AccA	−0.42	0.52	0.41	0.15	−0.18	FA–biosynthesis	
slr1511	FabH	−0.53	0.46	0.54	0.34	0.03		
sll1341	BfrA*	0.05	−0.13	−0.25	0.72	0.36	Fe-transport and binding	
slr1890	BfrB*	0.18	−0.35	−0.51	0.19	−0.43	Preference to ferrous iron	
slr1894	MrgA*	−0.02	1.05	1.10	2.15	2.12		
slr1392	FeoB*	−0.56	5.75	5.87	5.36	4.98		
sll1406	FhuA*	−0.28	9.56	9.62	9.43	9.40		
slr1295	FutA1*	−0.53	4.82	4.83	4.99	4.68	Preference to ferric iron	
slr0513	FutA2*	−0.53	4.62	4.72	5.11	5.24		
slr0327	FutB	−0.09	2.30	2.45	2.64	3.07		
sll1878	FutC	−0.33	3.98	4.09	4.03	4.54		
sll1454	NarB*	−0.47	−1.10	−1.05	−1.46	−1.14	Glutamate family / Nitrogen assimilation	
sll0209	Aar	−0.55	0.67	0.80	0.88	0.94	Hydrocarbon biosynthesis	
sll0208	Ado*	−0.02	−0.08	−0.12	−0.16	−0.36		
sll1221	HoxF*	−0.81	−3.03	−3.07	−2.61	−1.68	Hydrogenase	
sll1226	HoxH	−0.85	−0.29	−0.26	−0.61	−0.37		
sll1223	HoxU*	−0.50	−2.58	−2.44	−1.97	−1.48		
slr2143	CefD	−0.10	0.77	1.00	1.76	1.84	Iron–sulphur cluster biosynthesis	
slr0387	NifS	−0.64	1.13	1.30	2.26	2.35		
sll0088	SufR*	−2.36	2.08	−1.33	2.47	−0.98		
slr0074	SufB	2.45	0.45	0.83	0.57	0.41		
slr0075	SufC	3.26	0.20	0.69	0.53	0.96		
slr0076	SufD	2.75	0.51	0.92	0.63	0.95		
slr0077	SufS	2.86	0.36	0.91	0.66	1.22		
slr1417	SufA*	1.21	0.03	−0.19	0.25	0.21		
slr1239	PntA	0.02	0.15	0.33	0.58	0.47	NAD(P)–metabolism	
sll0567	Fur*	0.17	−2.46	−2.35	−1.27	−1.08	Regulatory functions	
sll1626	LexA	−0.08	0.38	0.46	0.98	0.96		
sll1423	NtcA	−0.09	0.52	0.48	1.49	1.45		
slr0653	SigA	0.01	−0.35	−0.44	−0.76	−1.13	RNA synthesis. modification. and DNA transcription	
sll0306	SigB	0.40	1.36	1.62	1.67	1.57		
sll0184	SigC	0.00	0.98	1.12	1.54	1.48		
ssl2982	Ycf61	0.13	0.15	0.24	0.02	0.04		
slr0963	Sir*	−0.31	0.29	0.37	0.38	0.35	Serine family / Sulfur assimilation	
sll1382	Fed2*	0.92	−2.16	−1.99	−2.71	−3.22	Soluble electron carriers	
slr0150	Fed4*	0.32	−2.09	−1.91	−1.96	−1.67		
slr0148	Fed5*	0.00	−0.82	−0.53	−0.94	−0.64		
sll0662	Fed7*	−0.57	−1.62	−1.84	−1.62	−2.30		
slr1562	GrxC	0.03	0.92	0.99	1.38	1.07	SS–bond reduction	
slr0600	NTR	−0.20	0.92	1.01	1.60	1.59		
slr1139	TrxA	−0.19	0.44	0.46	1.19	0.93		
slr0623	TrxA	0.09	0.25	0.57	1.13	1.06		
sll1057	TrxM2	−0.49	0.04	0.16	0.04	−0.14		
sll1621	Type II PrX	0.06	0.81	0.80	0.91	0.92		
slr2136	GcpE*	−0.48	0.03	0.06	0.05	0.04	Terpenoid/isoprene biosynthesis	
slr0348	IspH. LytB*	−0.15	0.09	0.17	0.94	0.79		
slr1329	AtpB	−0.19	0.13	0.05	0.31	−0.02	ATP synthase	
sll1031	CcmM	−0.41	0.59	0.45	0.37	0.53	CO2 fixation	
sll1734	CupA	−0.17	0.99	0.93	0.43	0.49		
slr2094	FbpI	−0.52	0.34	0.26	0.70	0.56		
sll1525	Prk	−0.43	0.10	0.06	0.52	0.10		

(*continued on next page*)

Table 3 (*continued*)

slr0009	RbcL	−1.06	1.32	1.16	1.45	1.50		Photosynthesis & carbon fixation
slr0342	PetB*	−0.03	−1.32	−1.53	−1.57	−2.04	Cytochrome b6/f complex	
sll1316	PetC1*	−0.07	−1.15	−1.22	−1.26	−1.70		
sll1521	Flv1*	−0.49	−0.63	−0.42	1.20	1.34	Detoxification	
sll0550	Flv3*	−0.32	−1.13	−1.15	0.49	0.48		
sll0223	NdhB	−0.08	−0.50	−0.56	−0.82	−1.02	NADH dehydrogenase	
sll0520	NdhI*	0.00	−2.06	−1.73	−1.66	−1.07		
slr1302	CupB	−0.07	−0.46	−0.30	0.12	−0.04	Other	
sll0247	IsiA	−0.47	11.05	11.09	11.84	11.53	Photosystem I	
slr1835	PsaB*	0.01	−1.83	−2.02	−3.55	−3.28		
ssl0563	PsaC*	0.09	−1.66	−1.67	−3.30	−2.97		
slr0737	PsaD	−0.02	−1.88	−1.96	−3.67	−3.51		
slr2033	RubA*	−0.08	0.44	0.47	0.74	0.45	PSI–biogenesis	
slr1963	Ocp	−0.05	1.78	2.00	2.83	2.80	Photosystem II	
sll1398	Psb28	0.00	−0.07	−0.17	−0.27	−0.56		
slr1311	PsbA2*	−0.13	−0.79	−0.99	−1.71	−2.36		
sll0849	PsbD*	−0.24	−1.44	−1.18	−2.08	−2.79		
ssr3451	PsbE*	0.00	−1.06	−1.13	−1.87	−2.66		
sll0427	PsbO	0.10	−0.67	−0.69	−1.51	−2.25		
slr2067	ApcA	−0.11	−0.76	−0.79	−0.94	−1.36	Phycobilisome (PBS)	
slr0335	ApcE	−0.23	−0.63	−0.69	−0.72	−1.15		
sll1578	CpcA	−0.27	−0.84	−0.84	−1.39	−2.27		
sll0813	CtaC	0.08	0.41	0.28	0.90	0.65	Respiratory terminal oxidases (RTO)	
slr2082	CtaDII*	−0.16	0.29	0.24	0.66	0.43		
slr1379	CydA	0.25	0.46	0.45	1.42	1.23		
ssl3044	*	0.10	−0.26	−0.13	0.42	0.46	Soluble electron carriers	
sll0248	IsiB	−0.56	10.40	10.55	9.90	9.36		
slr1643	PetH*	−0.32	−0.12	−0.06	0.03	−0.05		

depleted conditions (continuous white light 50 μmol photons m^{-2} s^{-1}, 1% (v/v) CO_2, 30 °C, BG-11 media with or without supplemented ferric ammonium citrate) (Fig. 4A). Culture absorption spectra of the Δ*sufR* mutant, measured at $OD_{750\ nm} = 1$, revealed an increase in the amount of carotenoids (seen as higher signal at 480 nm) and reduced phycobilisome (absorption peak at 626 nm) and chl *a* (absorption peak at 680 nm) content under all tested conditions (Fig. 4B). This difference became apparent in the long-term 12 days batch cultivation (long-term treatment), where the changes in pigment composition were more pronounced and the Δ*sufR* mutant culture was more brownish than that of the WT (Fig. 4C).

3.3. ΔsufR mutant analysis by SRM

To obtain a comprehensive view about changes occurring in the protein expression profile resulting from *sufR* deletion, we applied a recently developed SRM proteomics method for *Synechocystis* [37]. The analysis was performed to monitor the protein expression in the Δ*sufR* mutant and WT under iron sufficient and deprived conditions, both upon short-term growth when $OD_{750\ nm} = 1$ was reached and after a long-term growth of 12 days under iron deprived conditions. Altogether 94 pre-selected proteins were quantified with high sensitivity (>20 ms dwell time for each precursor-to-fragment ion transition) in the designed assays. The targets were selected to represent several metabolic processes, especially those related to photosynthesis and carbon metabolism as well as to iron and Fe-S cluster metabolism. The targets were divided into three functional categories; (i) photosynthesis and carbon fixation, (ii) other anabolic reactions/auxiliary metabolism and (iii) catabolism/amphibolic pathways, as described previously [37]. The SRM experiment details, including the transition list and raw files can be found from PASSEL [50] with a dataset identifier PASS00765 (http://www.peptideatlas.org/PASS/PASS00765) and the SRM results can be accessed in Panorama Public [51] as Skyline format (https://panoramaweb.org/labkey/SufR).

To differentiate the effects of *sufR* deletion from iron deprivation, all the tested conditions and strains were first compared against the WT strain under iron sufficient conditions (Table 3). The differential expression of the proteins in the Δ*sufR* mutant vs. WT under all applied experimental conditions can be found in Table 4. The detailed statistical

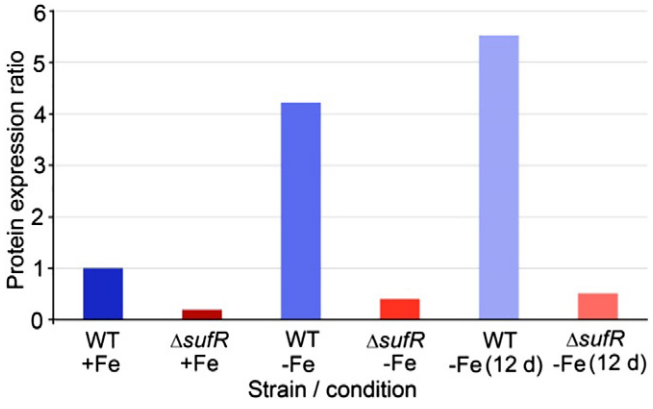

Fig. 2. SufR protein expression across all tested conditions and strains based on SRM-assays (adjusted p-values < 0.01). The signals observed in the mutant are considered as artefacts as they stem from truncated SufR protein. In the WT strain, the expression of SufR increased under iron depletion. The expression ratio is obtained by transforming the initial log_2 fold change values (Table 3) to simple fold change scale and compared against the WT + Fe-values normalized to 1.

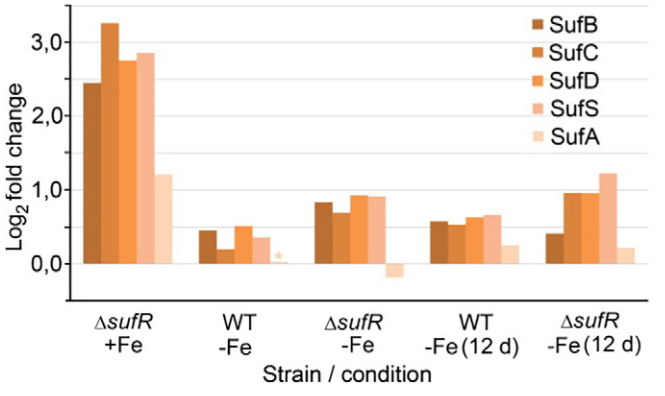

Fig. 3. Expression of the Suf proteins (SufBCDS and SufA) under iron sufficient and iron deprived growth conditions at log_2 scale (star indicates adjusted p-value > 0.01).

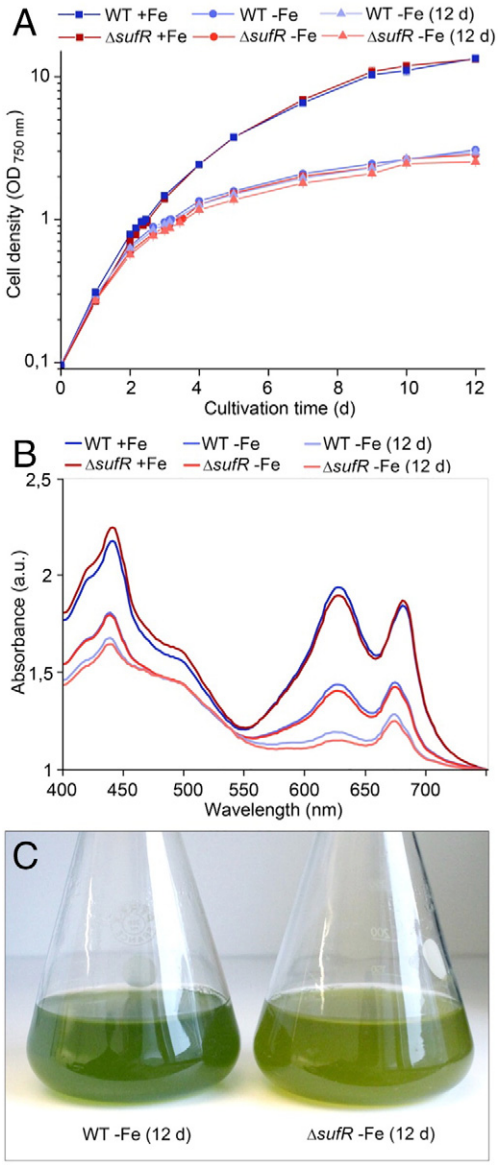

Fig. 4. A. Growth of *Synechocystis* WT and Δ*sufR* strain under tested conditions in logarithmic scale. The samples were collected at $OD_{750\ nm} = 1$ from both iron sufficient (squares) and iron deprived (circles) conditions and after 12 days (triangles) under iron deprivation. The cultures were grown at 1% (v/v) CO_2 atmosphere with white light illumination of 50 μmol photons m^{-2} s^{-1}. B. Absorbance spectra of *Synechocystis* WT and Δ*sufR* mutant cultures grown under iron sufficiency (+Fe) and iron deprived conditions (−Fe) at two different time points (at $OD_{750\ nm} = 1$ and on day 12). The spectra have been normalized to 750 nm. C. *Synechocystis* WT (left) and Δ*sufR* mutant (right) strains grown under iron deprived conditions for 12 days.

information on the expression level changes of all proteins under all the conditions is available in Table 3 in [43].

3.4. Highly induced iron-sulfur cluster biogenesis attenuates the expression of Fe-S proteins under iron sufficient conditions

The SufB (2.45, log_2 fold change), SufC (3.26), SufD (2.75) and SufS (2.86) proteins in addition to SufA (1.21) were all upregulated in the Δ*sufR* strain under iron sufficient conditions (Fig. 3; Δ*sufR* +Fe, Table 3; 1st data column), consistent with the known role of SufR as a repressor of the *suf* operon. This primary effect was accompanied by a downregulation of several enzymes harboring Fe-S clusters – a similar effect, although less pronounced, as observed under iron deprivation (Fig. 5A). The most downregulated Fe-S proteins included pyruvate flavodoxin oxidoreductase NifJ (−1.20), succinate dehydrogenase Fe-S protein SdhB (−1.12), diaphorase subunit HoxF (−0.81) (Fig. 5A; Δ*sufR* +Fe) and hydrogenase subunit HoxH (−0.85) of the bidirectional hydrogenase (Table 3; 1st data column). Significant downregulation was recorded also for proteins associated with i) CO_2 concentration and fixation including RbcL (Fig. 5B; Δ*sufR* + Fe), CcmM, CupA, FbpI and Prk, ii) O_2 photoreduction such as Flv1 and Flv3, and iii) light harvesting proteins CpcA (Fig. 5C; Δ*sufR* +Fe), ApcA and ApcE. The expression of proteins involved in iv) Fe-transport and binding including FutC, FeoB (Fig. 5B; Δ*sufR* +Fe), FutA1 and FutA2, v) pyruvate and acetyl-CoA metabolism such as NifJ (Fig. 5A; Δ*sufR* +Fe), Acs and Ppc, as well as vi) AccA and FabH in fatty acid metabolism followed a similar trend. The downregulation of many carbon fixation associated proteins was accompanied by an increased expression of the Fe-S protein glycolate dehydrogenase subunit, GlcF (Fig. 5D; Δ*sufR* +Fe). The glycolate dehydrogenase is a component of the photorespiratory pathway, which despite being essential [52], decreases the efficiency of carbon assimilation due to oxidation reaction in Rubisco [53].

3.5. Under short-term iron deprivation the inactivation of SufR induces only modest changes in global protein expression

All *suf* operon proteins were upregulated under short-term iron deprived conditions in the Δ*sufR* mutant, yet their expression was clearly lower in comparison to iron sufficient conditions (Fig. 3, Table 3; 1st and 3rd data column). Overall, under short-term iron deprivation ($OD_{750\ nm} = 1$) the *sufR* deletion had modest consequences on the expression level of the various target proteins. In comparison to the WT under the same conditions (Table 4; 2nd data column), the most affected proteins were the *suf* operon proteins (SufB; 0.38, SufC; 0.50, SufD; 0.41, SufS; 0.56), and the most upregulated protein was the glycolate dehydrogenase Fe-S subunit F, GlcF (1.31) (Fig. 5D) [52].

3.6. Long-term iron deprivation leads to elevated expression of Fe-S proteins in ΔsufR mutant

In accordance with the observed phenotypic changes in the Δ*sufR* mutant, the overall protein expression profile was altered more extensively in long-term iron deprivation than in short-term treatment ($OD_{750\ nm} = 1$) (Table 4; 2nd and 3rd data column). The clearest effects in comparison to the WT included diminished amounts of PSII-associated proteins, increased expression of Fe-S proteins and differential expression of complexes involved in ferrous (Fe^{2+}) and ferric (Fe^{3+}) iron transport. As in the short-term iron depletion experiment, the *suf* operon was induced also in the long-term treatment but only moderately (SufC; 0.43, SufD; 0.32, SufS; 0.56) (Table 4; 3rd data column).

Although all the photosynthetic complexes were greatly downregulated under long-term iron deprivation (Table 3; 4th and 5th data column), the relative amplitude of downregulation was different for proteins related to PSI and PSII between Δ*sufR* mutant and WT (Fig. 5C). The proteins of PSII (PsbE; −0.79, PsbO; −0.75, PsbD; −0.71, PsbA2; −0.65 and Psb28; −0.29), phycobilisome (CpcA; −0.88, ApcE; −0.43, ApcA; −0.42) and the iron rich cytochrome b_6f complex (PetB; −0.47 and PetC1; −0.44) were all downregulated in Δ*sufR*. On the contrary, the PSI proteins (PsaB; 0.26, PsaC; 0.33 and PsaD; 0.16) were repressed to a lower extent in the mutant than in the WT under long-term iron deprivation. (Table 4; 3rd data column)

In general, under iron deprived conditions the expression of the Fe-transport proteins was elevated in comparison to iron sufficient conditions in both strains (Table 3). In Δ*sufR* mutant, however, there was a decrease in the amount of ferrous iron transport and binding proteins, and an increase in ferric iron specific Fut-system in comparison to WT in the long-term treatment (Fig. 5B). In parallel to the downregulation of the ferrous iron transport protein FeoB (−0.38), the Alternative Respiratory Terminal Oxidase CtaDII (ARTO), which has been shown to

Table 4
The expression level fold changes of Δ*sufR* mutant vs. WT control strain. Log_2 scale upregulation and downregulation of the proteins are shown in red and green gradient, respectively. The values marked with small font indicate adjusted p-values >0.01. The asterisk (*) indicates that the respective protein binds either Fe or Fe-S-binding motifs based on UniProt and Cyanobase annotations and literature.

Gene	Protein symbol	I. ΔsufR vs. WT + Fe	II. ΔsufR vs. WT − Fe	III. ΔsufR vs. WT − Fe. 12d	Metabolic context/ function	Functional category
sll1831	GlcF*	0.32	1.31	0.60	Glycolate pathway	Catabolism/ amphibolic pathways
sll1196	PfkA	−0.01	0.22	−0.06	Glycolysis	
slr1843	Zwf	−0.32	0.16	−0.01	Pentose phosphate pathway	
sll0741	NifJ. Pfo*	−1.20	−0.35	0.14	Pyruvate and acetyl–CoA metabolism	
sll0542	Acs	−0.59	−0.10	−0.25		
sll0920	Ppc	−0.20	0.01	−0.26		
slr0665	AcnB*	−0.64	0.18	−0.15	TCA cycle	
slr1289	Icd	−0.19	−0.04	−0.01		
sll0823	SdhB*	−1.12	0.17	−0.04		
sll1625	SdhB*	−0.53	0.13	0.16		
sll0158	GlgB	−0.33	0.11	−0.02	Carbohydrate metabolism	Other anabolic reactions/ auxiliary metabolism
sll1356	GlgP*	−0.09	0.12	−0.16		
sll0169	ZipN. Ftn2	−0.04	0.06	−0.41	Cell division	
slr0417	GyrA	−0.44	0.14	−0.16	DNA unwinding	
sll0698	DspA/Hik33	−0.25	0.03	−0.05	Drug and analog sensitivity	
sll0728	AccA	−0.42	−0.11	−0.33	FA–biosynthesis	
slr1511	FabH	−0.53	0.08	−0.31		
sll1341	BfrA*	0.05	−0.12	−0.36	Fe –transport and binding	
slr1890	BfrB*	0.18	−0.17	−0.62		
slr1894	MrgA*	−0.02	0.06	−0.03		
slr1392	FeoB*	−0.56	0.12	−0.38		
sll1406	FhuA*	−0.28	0.06	−0.03		
slr1295	FutA1*	−0.53	0.01	−0.31		
slr0513	FutA2*	−0.53	0.10	0.13		
slr0327	FutB	−0.09	0.15	0.43		
sll1878	FutC	−0.33	0.11	0.51		
sll1454	NarB*	−0.47	0.05	0.32	Glutamate family / Nitrogen	
sll0209	Aar	−0.55	0.13	0.06	Hydrocarbon biosynthesis	
sll0208	Ado*	−0.02	−0.04	−0.20		
sll1221	HoxF*	−0.81	−0.05	0.93	Hydrogenase	
sll1226	HoxH	−0.85	0.02	0.24		
sll1223	HoxU*	−0.50	0.14	0.49		
slr2143	CefD	−0.10	0.23	0.08	Iron–sulphur cluster biosynthesis	
slr0387	NifS	−0.64	0.17	0.08		
sll0088	SufR*	−2.36	−3.40	−3.45		
slr0074	SufB	2.45	0.38	−0.16		
slr0075	SufC	3.26	0.50	0.43		
slr0076	SufD	2.75	0.41	0.32		
slr0077	SufS	2.86	0.56	0.56		
slr1417	SufA*	1.21	−0.22	−0.04		
slr1239	PntA	0.02	0.18	−0.11	NAD(P)–metabolism	
sll0567	Fur*	0.17	0.10	0.20	Regulatory functions	
sll1626	LexA	−0.08	0.08	−0.02		
sll1423	NtcA	−0.09	−0.04	−0.05		
slr0653	SigA	0.01	−0.09	−0.37	RNA synthesis. modification. and DNA transcription	
sll0306	SigB	0.40	0.26	−0.10		
sll0184	SigC	0.00	0.15	−0.06		
ssl2982	Ycf61	0.13	0.09	0.02		
slr0963	Sir*	−0.31	0.08	−0.03	Serine family / Sulfur assimilation	
sll1382	Fed2*	0.92	0.17	−0.50	Soluble electron carriers	
slr0150	Fed4*	0.32	0.18	0.29		
slr0148	Fed5*	0.00	0.29	0.30		
sll0662	Fed7*	−0.57	−0.22	−0.68		
slr1562	GrxC	0.03	0.06	−0.31	SS–bond reduction	
slr0600	NTR	−0.20	0.09	−0.01		
slr1139	TrxA	−0.19	0.02	−0.26		
slr0623	TrxA	0.09	0.32	−0.07		
sll1057	TrxM2	−0.49	0.13	−0.18		
sll1621	Type II PrX	0.06	0.00	0.01		

Fe –transport and binding: Preference to ferrous iron; Preference to ferric iron

Table 4 (*continued*)

slr2136	GcpE*	−0.48	0.02	−0.02	Terpenoid/isoprene biosynthesis	
slr0348	IspH. LytB*	−0.15	0.08	−0.15		
slr1329	AtpB	−0.19	−0.07	−0.33	ATP synthase	Photosynthesis & carbon fixation
sll1031	CcmM	−0.41	−0.14	0.16	CO2 fixation	
sll1734	CupA	−0.17	−0.06	0.06		
slr2094	FbpI	−0.52	−0.08	−0.14		
sll1525	Prk	−0.43	−0.04	−0.42		
slr0009	RbcL	−1.06	−0.15	0.05		
slr0342	PetB*	−0.03	−0.21	−0.47	Cytochrome b6/f complex	
sll1316	PetC1*	−0.07	−0.07	−0.44		
sll1521	Flv1*	−0.49	0.21	0.15	Detoxification	
sll0550	Flv3*	−0.32	−0.01	−0.01		
sll0223	NdhB	−0.08	−0.06	−0.20	NADH dehydrogenase	
sll0520	NdhI*	0.00	0.33	0.59		
slr1302	CupB	−0.07	0.15	−0.15	Other	
sll0247	IsiA	−0.47	0.04	−0.31	Photosystem I	
slr1835	PsaB*	0.01	−0.19	0.26		
ssl0563	PsaC*	0.09	−0.02	0.33		
slr0737	PsaD	−0.02	−0.08	0.16		
slr2033	RubA*	−0.08	0.03	−0.30	Photosystem I biogenesis	
slr1963	Ocp	−0.05	0.23	−0.03	Photosystem II	
sll1398	Psb28	0.00	−0.10	−0.29		
slr1311	PsbA2*	−0.13	−0.20	−0.65		
sll0849	PsbD*	−0.24	0.26	−0.71		
ssr3451	PsbE*	0.00	−0.07	−0.79		
sll0427	PsbO	0.10	−0.02	−0.75		
slr2067	ApcA	−0.11	−0.03	−0.42	Phycobilisome (PBS)	
slr0335	ApcE	−0.23	−0.06	−0.43		
sll1578	CpcA	−0.27	0.00	−0.88		
sll0813	CtaC	0.08	−0.13	−0.24	Respiratory terminal oxidases (RTO)	
slr2082	CtaDII*	−0.16	−0.05	−0.23		
slr1379	CydA	0.25	−0.01	−0.19		
ssl3044	*	0.10	0.13	0.04	Soluble electron carriers	
sll0248	IsiB	−0.56	0.15	−0.54		
slr1643	PetH*	−0.32	0.06	−0.09		

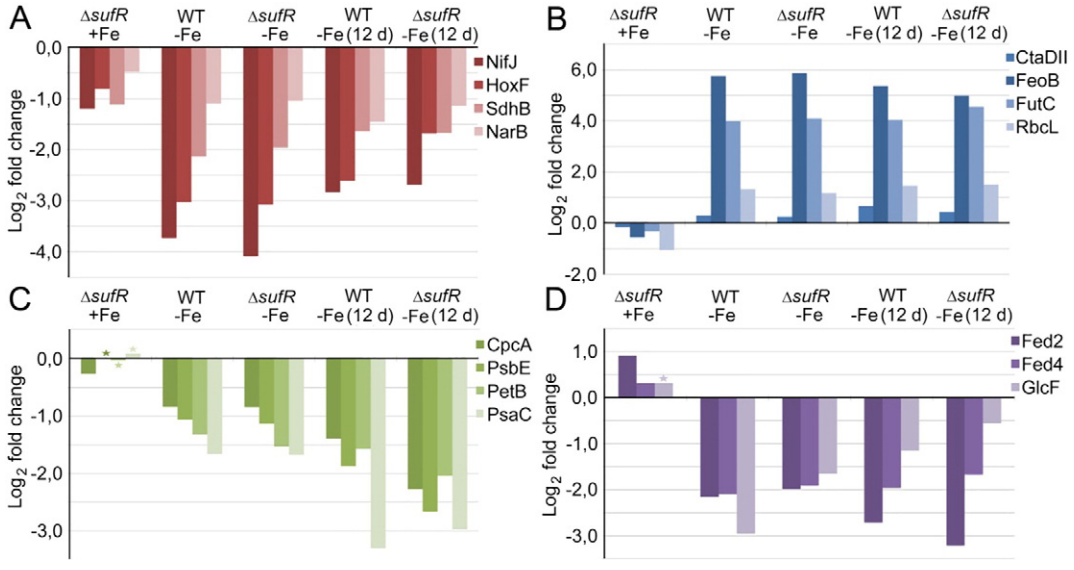

Fig. 5. Expression fold changes (Log_2FC) of selected representative proteins discussed in the text. A. Downregulation of Fe-S proteins was seen in Δ*sufR* mutant under iron sufficient conditions (+Fe) as well as under iron deprivation (−Fe). Under long-term iron deprivation [−Fe (12 days)] these Fe-S proteins were less repressed in the Δ*sufR* mutant in comparison to the WT. B. Proteins which have opposite expression trends in Δ*sufR* mutant under iron sufficient conditions (+Fe) in comparison to cells grown under iron deprivation. C. The effect of *sufR* deletion and iron deprivation on PSII and PSI associated proteins. D. Fed4 and GlcF represent mutant-specific expression trends (constant upregulation in comparison to WT), whereas Fed2 represents the condition-specific expression trends (regulation dependent on the growth conditions). The expression changes with adjusted p-values > 0.01 are marked with star.

participate in reductive iron uptake by FeoB [21], was likewise downregulated (−0.23) (Table 4; 3rd data column).

3.7. Identification of condition-independent and condition-specific changes in ΔsufR mutant

The SRM analysis revealed a set of proteins responding similarly to the deletion of the *sufR* gene across all experimental conditions used in this study (*mutation-specific* response). In addition to the characteristic upregulation of the *suf* operon, these expression trends involved alleviated repression of glycolate dehydrogenase subunit F (GlcF) and a ferredoxin, petF-like protein (Fed4) (Fig. 5D), as well as the downregulation of fatty acid biosynthesis, carbon fixation (Prk) and phycobilisome (CpcA) proteins in comparison to the WT strain under corresponding conditions (Table 4).

Another set of proteins demonstrated protein expression trends in which the response of the Δ*sufR* strain was dependent primarily on the iron conditions (*condition-specific* response). This group involved proteins harboring Fe-S clusters such as HoxF, NarB (Fig. 5A) and HoxU, in addition to FutC related to Fe (III)-transport (Fig. 5B). Under iron sufficient conditions these proteins in the Δ*sufR* mutant were consistently downregulated, whereas under iron deprivation the effect was opposite in comparison to the WT strain under corresponding conditions (Table 4). Fed2 was the only protein out of the 94 targets for which the condition-specific response was the other way around, and the protein was expressed at higher levels in the presence of iron and repressed in the absence of iron as compared to the WT (Table 4).

3.8. SufR deletion does not induce changes in the relative ratio of functional PSII/PSI complexes

The relative ratios of functional PSI and PSII reaction centers in the Δ*sufR* mutant and the WT control strain were analyzed using EPR spectroscopy (Fig. 6). The EPR signal I (dotted line) corresponds to oxidized $P700^+$ representing the amount of active PSI, while the signal II (solid line) corresponds to the oxidized tyrosine D ($Tyr D^{\bullet}$) which correlates with the amount of active PSII. The EPR profiles of oxidized $P700^+$ and $Tyr D^{\bullet}$ did not change in response to *sufR* deletion under iron sufficient conditions (Fig. 6A) or under long-term iron deprived conditions (Fig. 6B). In the presence of iron, the PSI/PSII ratios were 4.31 ± 0.68 and 4.69 ± 0.71 for the WT and the Δ*sufR* mutant, respectively (Fig. 6C; bright blue and red bars). Under the iron deprived conditions, the total content of functional PSI was drastically reduced in both strains as seen in the relative decline in signal intensity of $P700^+$ (Fig. 6A & B). The functional PSI/PSII ratio decreased by several folds to 0.54 ± 0.13 and 0.50 ± 0.13, in WT and in Δ*sufR* mutant, respectively. (Fig. 6C)

3.9. RT-qPCR verifies the direct targets for SufR regulation

In order to evaluate whether the protein level changes observed in *sufR* deletion strain are seen already at the transcript level, and thus could be verified as direct targets for the SufR regulation, we performed RT-qPCR for several genes encoding proteins with altered expression. The targets included genes for proteins with a *mutation-specific* expression i.e. Fed4 (*slr0150*) and SufB (*slr0074*), a *condition-specific* expression i.e. Fed2 (*sll1382*), and an altered expression under iron sufficient conditions i.e. NifJ (*sll0741*) and SdhB (*sll0823*). In addition, the transcript accumulation for SufR (*sll0088*) and SyNifU [54] (*ssl2667*) was analyzed. SyNifU could not be targeted in SRM assays due to lack of PTPs, but the corresponding transcript levels were measured as the protein has been proposed to function as a scaffold for Fe-S cluster assembly and transport [54]. In the case of *fed2*, *fed4* and *sdhB*, the relative transcript abundances were not noticeably affected (Fig. 7), and to some extent the expression trends were even the opposite in comparison to the SRM results under the tested conditions. This implies that the expression changes observed at protein level were indirect effects of the SufR inactivation. Furthermore, the relative transcript accumulation of *synifU* proved to be negligible in the *sufR* deletion strain. On the contrary, *sufB* and *nifJ* showed similar expression trends both on the transcript and the protein levels, suggesting them to be direct targets of SufR regulation (the *sufB* transcript accumulation under long term iron deprivation being the only exception). The relative transcript abundance of *nifJ* was 0.48 ± 0.08 ($log_2FC = -1.05$) under iron sufficient conditions, which is comparable to the amplitude of downregulation at the protein level ($log_2FC = -1.20$). Similar correlation was seen under the two iron deprived conditions, although the amplitude of regulation was not as high as under iron sufficiency (Fig. 7 and Table 4). RT-qPCR also verified the

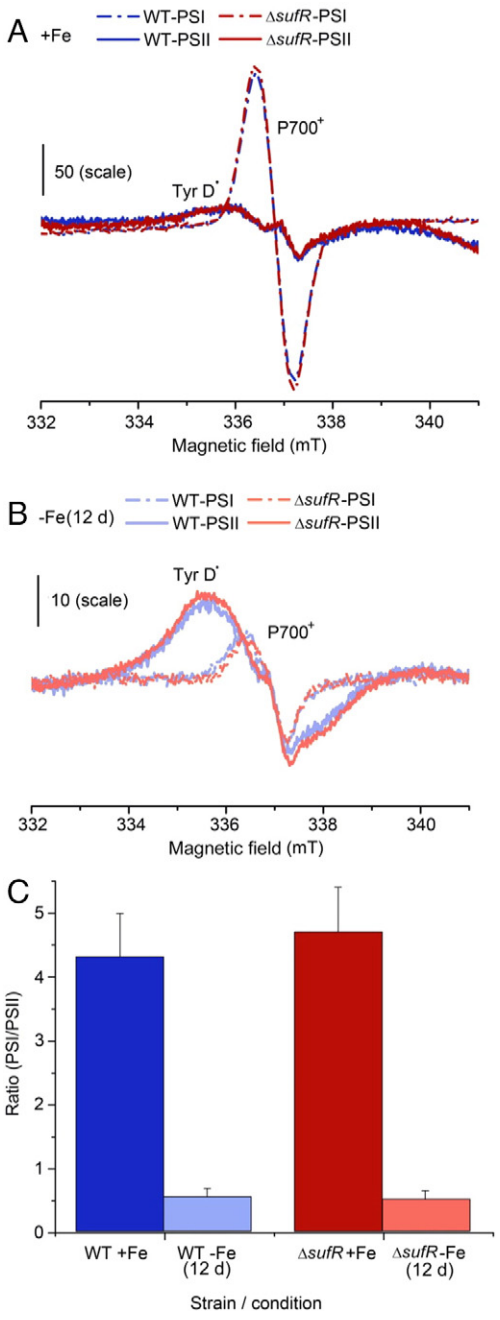

Fig. 6. Quantification of functional PSII and PSI reaction centers in *Synechocystis* using EPR spectroscopy. Overlay of oxidized $P700^+$ and $TyrD^{\bullet}$ EPR spectra from WT and Δ*sufR* mutant under A) iron sufficient culture conditions (+Fe) and B) iron deprived culture conditions (−Fe). C) PSI/PSII ratios of WT and Δ*sufR* mutant in the presence of iron (bright blue and red, respectively) and in the absence of iron (light blue and red, respectively) calculated from A) and B) on basis of chl *a*.

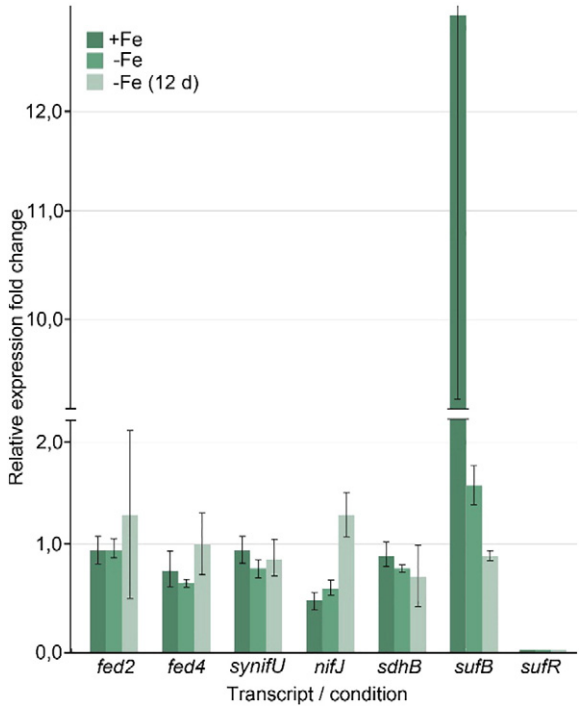

Fig. 7. Transcript accumulation of *fed2*, *fed4*, *synifU*, *nifJ*, *sdhB*, *sufB* and *sufR* in the *sufR* deletion strain under the applied experimental conditions as analyzed with RT-qPCR. The bars with three-color gradient from dark to light green represent iron sufficient (+Fe), short-term iron deprived (−Fe) and long-term iron deprived [−Fe (12 days)] conditions, respectively. The results are the means from three biological replicates with standard deviations.

sufR deletion with transcript accumulation being similar or lower than in the negative controls.

4. Discussion

4.1. New protein level insight on the effects of SufR by targeted proteomics

SufR is a negative transcriptional regulator of the *suf* operon involved in the synthesis of Fe-S clusters [30,35,55,56], and of specific interest in photosynthetic oxygen evolving cyanobacteria which are highly dependent on these cofactors. SufR was first discovered through screening of viable suppressor mutations for primary mutations in *psaC*, which substituted cysteine ligand for [4Fe-4S] cluster, F_B, with serine ($C14S_{PsaC}$) in the PSI protein PsaC [57]. The mutations inactivating *sufR* enabled photoautotrophic growth and restored the amounts of mutated PsaC to WT levels [55]. The role of SufR has been further investigated in cyanobacteria [30,58], but prior to this work, the direct and secondary effects have not been studied at protein level, or in response to the availability of iron in the model organism *Synechocystis*. Here we generated a SufR deficient *Synechocystis* mutant strain, and deployed SRM proteomics for monitoring protein-level changes arising either directly from the deletion itself or from the altered regulation of Fe-S cluster metabolism via the *suf* operon and *nif*. Our SRM analysis of the Δ*sufR* mutant also enabled the screening of the changes occurring under iron sufficient and deprived conditions in processes that are either directly or indirectly linked to Fe-S cluster metabolism, with a specific focus on the iron-rich proteins associated with photosynthetic apparatus and selected key metabolic processes of the host. Since these effects and interactions could otherwise be challenging to identify, SRM provided a convenient and comprehensive means to elucidate the functional role of SufR more extensively.

4.2. Suf operon regulation

The *suf* operon response observed under iron deprived culture conditions in the WT was consistent with [4Fe-4S]-cluster demetallation of SufR i.e. transition from holo- to apo-form and consequent *suf* operon derepression [30]. However, in the Δ*sufR* mutant, the extent of the *suf* operon induction was notably higher than in WT, reflecting a more complete derepression of the operon in the absence of SufR under all tested conditions (Fig. 3). Interestingly, the expression of the Suf proteins in *Synechocystis* Δ*sufR* mutant was clearly lower under iron depletion than under iron sufficient conditions, in contrast to the *Synechococcus* Δ*sufR* mutant, where strong and constitutive upregulation of the *suf* operon transcripts was observed under both conditions [30].

Observation of a lower induction of Suf proteins and *sufB* transcription in *Synechocystis* Δ*sufR* mutant in the absence of iron than in iron sufficiency suggests that there may be some SufR-independent regulatory mechanism controlling the translation of the *suf* operon and mRNA degradation under iron depletion in *Synechocystis*. Such regulation could involve a small non-coding RNA (sRNA), predicted within the 5′ UTR of *sufB* gene [59], and a promoter with a transcriptional start site at position 2871555 (120 nt upstream of the *sufB* start codon), which becomes highly induced especially during iron deprivation [60]. As the region overlaps with the regulatory site of the *suf* operon [31], it could affect the transcription of the downstream *suf* genes. It is likewise conceivable that the *suf* operon expression is controlled via a *mixed regulatory circuit* [61], including a combined effect of a transcription factor and sRNA as a post-transcriptional regulator, thus resembling the regulation of ErpA in *Escherichia coli*. In this system, both the transcription factor IscR and sRNA RyhB repress the expression of an Fe-S cluster carrier protein ErpA, however, under different iron concentrations [62]. Moreover, the expression of the *isc* operon, which codes for proteins involved in the assembly of a housekeeping Fe-S cluster system in *E. coli*, has been shown to be regulated by the combination of the transcription factor IscR [63] and non-coding RNA RyhB [64], with the recruitment of the regulator being dependent on the availability of iron. It is thus apparent that protein expression associated with Fe-S cofactor assembly involves complex and fine-tuned control systems even in heterotrophic organisms, and this is likely to apply also for autotrophic bacteria such as *Synechocystis* which are even more dependent on the precise modulation of iron metabolism under changing environmental conditions.

4.3. Protein-level responses to suf operon induction

The observed protein level consequences associated with Suf protein expression vary depending on the amount of available iron. In *Synechococcus*, the induction of *sufBCDS* genes resulted in growth inhibition under iron sufficient conditions, whereas under iron depletion the induced transcription of *suf* genes has been linked to enhanced ability to grow [30]. Accordingly, on the basis of our data, the *sufR* deletion appeared to have a negative impact on *Synechocystis* under iron sufficient conditions: Although the growth of the Δ*sufR* mutant was not affected (Fig. 4A), the Fe-S proteins were downregulated, phycobilisome absorbance was decreased, and the stress responsive carotenoid pigments were more abundant than in the control strain (Fig. 4B). Thus, in the presence of iron, when the Suf protein expression is not induced in the native cells, deletion of the SufR repressor results in uncontrolled Fe-S cluster biogenesis. This is accompanied by the downstream effects which resemble iron deprivation such as downregulation of Fe-S proteins. Certain Fe-S proteins, however, were not regulated the same way as in response to iron deprivation, emphasizing the difference between SufR-specific and condition-specific effects in the absence of iron. For example, the expression of PSI subunits PsaB (one [4Fe-4S] cluster) and PsaC (two [4Fe-4S] clusters) was not altered at all, whilst Fed2 and Fed4, both harboring [2Fe-2S] clusters, showed elevated expression levels in the mutant. This was proven to be an indirect consequence of the *sufR* deletion, as the change in the expression of *fed2* and *fed4* at the transcript level was negligible (Fig. 7).

Under iron depletion the Suf proteins were only moderately upregulated in the Δ*sufR* mutant, with concurrent minimal impact also on the expression of other proteins. Hence, the effects caused by *sufR* deletion were largely masked by the changes induced by iron deprivation. In some cases the difference between the Δ*sufR* strain and WT appeared only after long-term iron deprivation, as in the case of Fe-S cluster proteins. For example, while the PSI and PSII complexes were increasingly downregulated in the course of iron depletion (Fig. 5C), the Fe-S cluster proteins of the PSI complex as well as other Fe-S proteins (HoxF, GlcF; Fig. 5A & D) were less repressed in the mutant. On the other hand, the PSII associated proteins were found to be systematically more repressed in the mutant than in WT.

In parallel to SRM, EPR spectroscopy was applied to evaluate (i) if the higher amount of PSI proteins in the Δ*sufR* strain under iron deprivation resulted in increased levels of *functional* PSI complexes, and (ii) if the simultaneous downregulation of PSII proteins could be seen as changes in relative functionality of the photosystems. The results demonstrated no significant change in the relative quantities of functional photosystems between the Δ*sufR* mutant and the WT (Fig. 6). This suggests that the slight accumulation of PSI-associated proteins does not contribute to the amount of active PSI complexes when iron is not readily available. Thus, although the Fe-S cluster biogenesis and repair machinery is activated, the limited amount of iron results in an accumulation of catalytically inactive proteins in the mutant with consequences on the repression of PSII proteins. This is in full accordance with the strict requirement of redox balance upon functioning of the photosynthetic apparatus and with the suggested mechanism of the PSI centers depleted of Fe-S clusters functioning as photoprotective energy quenchers capable of dissipating excess energy from the photosynthetic apparatus under stress conditions [65]. Despite increased need of iron for the Fe-S cluster proteins in the Δ*sufR* mutant, there is a decrease in the proteins involved in Fe^{2+} specific transport system, which is only partially compensated by the upregulation of the less effective Fe^{3+} specific Fut-transport system (Fig. 5B) [21].

4.4. New roles of SufR

Our SRM analysis provided evidence suggesting that SufR affects the protein expression profile also by other means than via repression of the *suf* operon. This is supported by the comparative genome analysis by RegPrecise 3.0 [66], which implicate that there are three different regulons for SufR; SufR itself, the *suf* operon and NifJ, an Fe-S cluster protein with a central role in carbon metabolism. NifJ is a pyruvate:ferredoxin oxidoreductase (PFOR) which catalyzes the conversion of pyruvate into acetyl-CoA [67], thus affecting the metabolic flux towards acetyl-CoA-derived products. The observed NifJ downregulation in the Δ*sufR* mutant under iron sufficient conditions, as observed both at the protein and the transcript level, likely explains the observed downregulation of the proteins involved in the downstream processes from acetyl-CoA (Table 3; 1st data column). These include proteins taking part in the biosynthesis of lipids (AccA; −0.42 and FabH; −0.53), terpenoids (GcpE; −0.48 and IspH; −0.15), flavonoids, polyketides, amino acids (glutamate, glutamine, proline, arginine), and other precursor molecules produced in the TCA cycle (AcnB; −0.64, Icd; −0.19, SdhB encoded by *sll0823*; −1.12 and SdhB encoded by *sll1625*; −0.53). The regulation of NifJ thus corroborates the hypothesis that SufR could be associated with some non-photosynthetic housekeeping processes and possibly in some contexts required for viability, as supported by the fact that some previous attempts to delete *sufR* from *Synechocystis* have failed [30,55].

5. Conclusion

The regulation of Fe-S cluster biogenesis by the transcriptional repressor SufR is highly dependent on the amount of available iron in the cyanobacterial model organism *Synechocystis* sp. PCC 6803. Under iron sufficient conditions, SufR is the main repressor of the *suf* operon as well as an activator of NifJ, and apparently associated with maintaining the physiological levels of Fe-S proteins in the cell. Under iron deprivation, the *suf* operon is induced due to de-repression of apo-SufR, but the expression of *suf* operon appears to be regulated also independently of SufR. This tight control is physiologically important when iron is not readily available for the Fe-S cluster biosynthesis. Our results suggest that in the absence of native SufR regulation the induced *suf* operon would lead to accumulation of inactive proteins devoid of Fe-S cofactors.

Transparency document

The Transparency document associated with this article can be found, in the online version.

Acknowledgements

This work was financially supported by the Academy of Finland [grants #253269, #272424, #307335 and #273870] and Tekes [grant #40128/14]. The Biocenter Finland and the Proteomics Facility of the Turku Centre for Biotechnology are acknowledged for the support in MS-analysis.

Appendix A

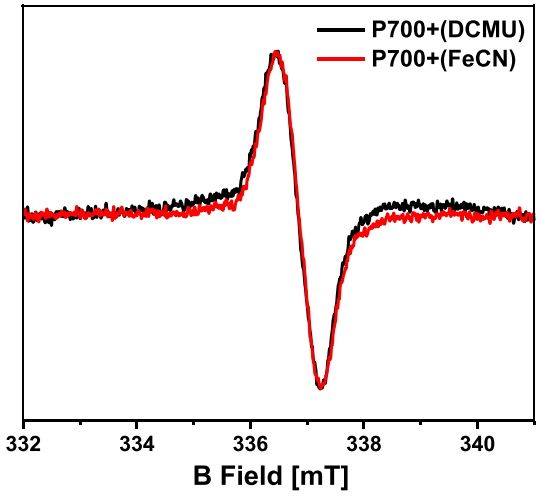

Appendix Fig. A.1. Overlay of EPR spectra obtained from WT *Synechocystis* cells treated with DCMU (10 μM; black line) and FeCN (100 mM; red line), representing fully oxidized P700 reaction centers. The data was recorded from cells cultivated under iron sufficient conditions.

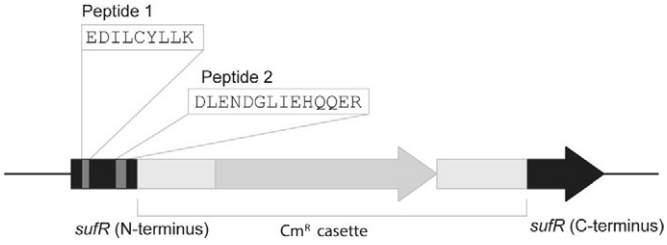

Appendix Fig. A.2. The constructed *sufR*::Cm^R disruption strain. Representation of *sufR* gene (black) inactivated by insertion of a chloramphenicol resistance cassette (light grey) encoding for heterologous chloramphenicol acetyltransferase in *Synechocystis*. The only suitable SufR specific PTPs fulfilling the criteria for SRM analysis correspond to sequences encoded by the 5′ end of *sufR* (Peptides 1–2).

References

[1] T.A. Rouault, W.-H. Tong, Iron-sulphur cluster biogenesis and mitochondrial iron homeostasis, Nat. Rev. Mol. Cell Biol. 6 (2005) 345–351.
[2] P. Fromme, I. Grotjohann, Structural analysis of cyanobacterial photosystem I, in: J.H. Golbeck (Ed.) Photosystem I: The Light-driven Plastocyanin: Ferredoxin Oxidoreductase. Advances in Photosynthesis and Respiration, vol. 24, Springer 2006, pp. 47–69.
[3] G. Hauska, E. Hurt, N. Gabellini, W. Lockau, Comparative aspects of quinol-cytochrome c/plastocyanin oxidoreductases, Biochim. Biophys. Acta 726 (1983) 97–133.
[4] D. Schneider, S. Skrzypczak, S. Anemüller, C.L. Schmidt, A. Seidler, M. Rögner, Heterogeneous Rieske proteins in the cytochrome b_6f complex of *Synechocystis* PCC6803? J. Biol. Chem. 277 (2002) 10949–10954.
[5] S. Ouchane, W. Nitschke, P. Bianco, A. Vermeglio, C. Astier, Multiple Rieske genes in prokaryotes: exchangeable Rieske subunits in the cytochrome bc-complex of Rubrivivax gelatinosus, Mol. Microbiol. 57 (2005) 261–275.
[6] H. Beinert, P.J. Kiley, Fe-S proteins in sensing and regulatory functions, Curr. Opin. Chem. Biol. 3 (1999) 152–157.
[7] A. Latifi, R. Jeanjean, S. Lemeille, M. Havaux, C.C. Zhang, Iron starvation leads to oxidative stress in *Anabaena* sp. strain PCC 7120, J. Bacteriol. 187 (2005) 6596–6598.
[8] D. Petering, J.A. Fee, G. Palmer, The oxygen sensitivity of spinach ferredoxin and other iron-sulfur proteins. The formation of protein-bound sulfur-zero, J. Biol. Chem. 246 (1971) 643–653.
[9] S. Varghese, Y. Tang, J.A. Imlay, Contrasting sensitivities of *Escherichia coli* aconitases A and B to oxidation and iron depletion, J. Bacteriol. 185 (2003) 221–230.
[10] A.E. McDermott, V.K. Yachandra, R.D. Guiles, K. Sauer, M.P. Klein, K.G. Parrett, J.H. Golbeck, EXAFS structural study of FX, the low-potential Fe-S center in photosystem I, Biochemistry 28 (1989) 8056–8059.
[11] P.R. Chitnis, Photosystem I: function and physiology, Annu. Rev. Plant Physiol. Plant Mol. Biol. 52 (2001) 593–626.
[12] A. Zouni, H.-T. Witt, J. Kern, P. Fromme, N. Krauss, W. Saenger, P. Orth, Crystal structure of photosystem II from *Synechococcus elongatus* at 3.8 [angst] resolution, Nature 409 (2001) 739–743.
[13] N. Kamiya, J.R. Shen, Crystal structure of oxygen-evolving photosystem II from *Thermosynechococcus vulcanus* at 3.7-A resolution, Proc. Natl. Acad. Sci. U. S. A. 100 (2003) 98–103.
[14] G. Kurisu, H. Zhang, J.L. Smith, W.A. Cramer, Structure of the cytochrome b6f complex of oxygenic photosynthesis: tuning the cavity, Science 302 (2003) 1009–1014.
[15] D. Stroebel, Y. Choquet, J.-L. Popot, D. Picot, An atypical haem in the cytochrome b6f complex, Nature 426 (2003) 413–418.
[16] L.A. Finney, T.V. O'Halloran, Transition metal speciation in the cell: insights from the chemistry of metal ion receptors, Science 300 (2003) 931–936.
[17] N. Keren, R. Aurora, H.B. Pakrasi, Critical roles of bacterioferritins in iron storage and proliferation of cyanobacteria, Plant Physiol. 135 (2004) 1666–1673.
[18] S. Shcolnick, T.C. Summerfield, L. Reytman, L.A. Sherman, N. Keren, The mechanism of iron homeostasis in the unicellular cyanobacterium *Synechocystis* sp. PCC 6803 and its relationship to oxidative stress, Plant Physiol. 150 (2009) 2045–2056.
[19] B. Remes, B.A. Berghoff, K.U. Förstner, G. Klug, Role of oxygen and the OxyR protein in the response to iron limitation in *Rhodobacter sphaeroides*, BMC Genomics 15 (2014) 794.
[20] H.-B. Jiang, W.-J. Lou, W.-T. Ke, W.-Y. Song, N.M. Price, B.-S. Qiu, New insights into iron acquisition by cyanobacteria: an essential role for ExbB-ExbD complex in inorganic iron uptake, ISME J. 9 (2015) 297–309.
[21] C. Kranzler, H. Lis, O.M. Finkel, G. Schmetterer, Y. Shaked, N. Keren, Coordinated transporter activity shapes high-affinity iron acquisition in cyanobacteria, ISME J. 8 (2014) 409–417.
[22] D.E. Laudenbach, M.E. Reith, N.A. Straus, Isolation, sequence analysis, and transcriptional studies of the flavodoxin gene from *Anacystis nidulans* R2, J. Bacteriol. 170 (1988) 258–265.
[23] J.A. Ihalainen, S. D'Haene, N. Yeremenko, H. van Roon, A.A. Arteni, E.J. Boekema, R. van Grondelle, H.C. Matthijs, J.P. Dekker, Aggregates of the chlorophyll-binding protein IsiA (CP43′) dissipate energy in cyanobacteria, Biochemistry 44 (2005) 10846–10853.
[24] N. Yeremenko, R. Kouril, J.A. Ihalainen, S. D'Haene, N. van Oosterwijk, E.G. Andrizhiyevskaya, W. Keegstra, H.L. Dekker, M. Hagemann, E.J. Boekema, et al., Supramolecular organization and dual function of the IsiA chlorophyll-binding protein in cyanobacteria, Biochemistry 43 (2004) 10308–10313.
[25] T.S. Bibby, J. Nield, J. Barber, Iron deficiency induces the formation of an antenna ring around trimeric photosystem I in cyanobacteria, Nature 412 (2001) 743–745.
[26] D.E. Laudenbach, N.A. Straus, Characterization of a cyanobacterial iron stress-induced gene similar to psbC, J. Bacteriol. 170 (1988) 5018–5026.
[27] P.M. Wood, Interchangeable copper and iron proteins in algal photosynthesis. Studies on plastocyanin and cytochrome c-552 in *Chlamydomonas*, Eur. J. Biochem. 87 (1978) 9–19.
[28] G. Sandmann, P. Boger, Physiological factors determining formation of plastocyanin and plastidic cytochrome c-553 in *Scenedesmus*, Planta 147 (1980) 330–334.
[29] F.W. Outten, E.C. Theil, Iron-based redox switches in biology, Antioxid. Redox Signal. 11 (2009) 1029–1046.
[30] T. Wang, G. Shen, R. Balasubramanian, L. McIntosh, D.A. Bryant, J.H. Golbeck, The sufR gene (sll0088 in *Synechocystis* sp. strain PCC 6803) functions as a repressor of the sufBCDS operon in iron-sulfur cluster biogenesis in cyanobacteria, J. Bacteriol. 186 (2004) 956–967.
[31] G. Shen, R. Balasubramanian, T. Wang, Y. Wu, L.M. Hoffart, C. Krebs, D.A. Bryant, J.H. Golbeck, SufR coordinates two [4Fe-4S]2+, 1+ clusters and functions as a transcriptional repressor of the sufBCDS operon and an autoregulator of sufR in cyanobacteria, J. Biol. Chem. 282 (2007) 31909–31919.
[32] F.W. Outten, M.J. Wood, F.M. Munoz, G. Storz, The SufE protein and the SufBCD complex enhance SufS cysteine desulfurase activity as part of a sulfur transfer pathway for Fe-S cluster assembly in *Escherichia coli*, J. Biol. Chem. 278 (2003) 45713–45719.
[33] F.W. Outten, O. Djaman, G. Storz, A suf operon requirement for Fe-S cluster assembly during iron starvation in *Escherichia coli*, Mol. Microbiol. 52 (2004) 861–872.
[34] T. Clausen, J.T. Kaiser, C. Steegborn, R. Huber, D. Kessler, Crystal structure of the cystine C-S lyase from *Synechocystis*: stabilization of cysteine persulfide for FeS cluster biosynthesis, Proc. Natl. Acad. Sci. U. S. A. 97 (2000) 3856–3861.
[35] L. Nachin, L. Loiseau, D. Expert, F. Barras, SufC: an unorthodox cytoplasmic ABC/ATPase required for [Fe-S] biogenesis under oxidative stress, EMBO J. 22 (2003) 427–437.
[36] R. Rippka, J. Deruelles, J.B. Waterbury, M. Herdman, R.Y. Stanier, Generic assignments, strain histories and properties of pure cultures of cyanobacteria, Microbiology 111 (1979) 1–61.
[37] L. Vuorijoki, J. Isojärvi, P. Kallio, P. Kouvonen, E.M. Aro, G.L. Corthals, P.R. Jones, D. Muth-Pawlak, Development of a quantitative SRM-based proteomics method to study iron metabolism of *Synechocystis* sp. PCC 6803, J. Proteome Res. 15 (2016) 266–279.
[38] E. Szewczyk, T. Nayak, C.E. Oakley, H. Edgerton, Y. Xiong, N. Taheri-Talesh, S.A. Osmani, B.R. Oakley, B. Oakley, Fusion PCR and gene targeting in *Aspergillus nidulans*, Nat. Protoc. 1 (2006) 3111–3120.
[39] M.M. Bradford, A rapid and sensitive method for the quantitation of microgram quantities of protein utilizing the principle of protein-dye binding, Anal. Biochem. 72 (1976) 248–254.
[40] B. MacLean, D.M. Tomazela, N. Shulman, M. Chambers, G.L. Finney, B. Frewen, R. Kern, D.L. Tabb, D.C. Liebler, M.J. MacCoss, Skyline: an open source document editor for creating and analyzing targeted proteomics experiments, Bioinformatics 26 (2010) 966–968.
[41] M. Choi, C.Y. Chang, T. Clough, D. Broudy, T. Killeen, B. MacLean, O. Vitek, MSstats: an R package for statistical analysis of quantitative mass spectrometry-based proteomic experiments, Bioinformatics 30 (2014) 2524–2526.
[42] M. Choi, C. Chang, O. Vitek, MSstats: Protein Significance Analysis in DDA, SRM and DIA for Label-free or Label-based Proteomics Experiments. R Package Version 2.6.0, 2014 (Edited by).
[43] L. Vuorijoki, P. Kallio, E.M. Aro, SRM dataset of the proteome of inactivated iron-sulfur cluster biogenesis regulator SufR in Syn*echocystis* sp. PCC 6803, Data Brief (2017) (submitted for publication).
[44] J.C. Meeks, R.W. Castenholz, Growth and photosynthesis in an extreme thermophile, *Synechococcus lividus* (Cyanophyta), Arch. Mikrobiol. 78 (1971) 25–41.
[45] A. Tiwari, A. Jajoo, S. Bharti, Heat-induced changes in the EPR signal of tyrosine D (Y(D)OX) a possible role of Cytochrome b559, J. Bioenerg. Biomembr. 40 (2008) 237–243.
[46] A. Tiwari, A. Jajoo, S. Bharti, Heat-induced changes in photosystem I activity as measured with different electron donors in isolated spinach thylakoid membranes, Photochem. Photobiol. Sci. 7 (2008) 485–491.
[47] H. Mustila, P. Paananen, N. Battchikova, A. Santana-Sánchez, D. Muth-Pawlak, M. Hagemann, E.M. Aro, Y. Allahverdiyeva, The flavodiiron protein Flv3 functions as a homo-oligomer during stress acclimation and is distinct from the Flv1/Flv3 hetero-oligomer specific to the O_2 photoreduction pathway, Plant Cell Physiol. 57 (2016) 1468–1483.
[48] T. Tyystjärvi, M. Herranen, E.M. Aro, Regulation of translation elongation in cyanobacteria: membrane targeting of the ribosome nascent-chain complexes controls the synthesis of D1 protein, Mol. Microbiol. 40 (2001) 476–484.
[49] M.W. Pfaffl, A new mathematical model for relative quantification in real-time RT-PCR, Nucleic Acids Res. 29 (2001), e45. .
[50] T. Farrah, E.W. Deutsch, R. Kreisberg, Z. Sun, D.S. Campbell, L. Mendoza, U. Kusebauch, M.Y. Brusniak, R. Hüttenhain, R. Schiess, et al., PASSEL: the PeptideAtlas SRM experiment library, Proteomics 12 (2012) 1170–1175.
[51] V. Sharma, J. Eckels, G.K. Taylor, N.J. Shulman, A.B. Stergachis, S.A. Joyner, P. Yan, J.R. Whiteaker, G.N. Halusa, B. Schilling, et al., Panorama: a targeted proteomics knowledge base, J. Proteome Res. 13 (2014) 4205–4210.
[52] M. Eisenhut, W. Ruth, M. Haimovich, H. Bauwe, A. Kaplan, M. Hagemann, The photorespiratory glycolate metabolism is essential for cyanobacteria and might have been conveyed endosymbiontically to plants, Proc. Natl. Acad. Sci. U. S. A. 105 (2008) 17199–17204.
[53] W.L. Ogren, G. Bowes, Ribulose diphosphate carboxylase regulates soybean photorespiration, Nat. New Biol. 230 (1971) 159–160.
[54] K. Nishio, M. Nakai, Transfer of Iron-Sulfur Cluster from NifU to Apoferredoxin, J. Biol. Chem. 275 (2000) 22615–22618.
[55] J. Yu, G. Shen, T. Wang, D.A. Bryant, J.H. Golbeck, L. McIntosh, Suppressor mutations in the study of photosystem I biogenesis: *sll0088* is a previously unidentified gene involved in reaction center accumulation in *Synechocystis* sp. strain PCC 6803, J. Bacteriol. 185 (2003) 3878–3887.
[56] Y. Takahashi, U. Tokumoto, A Third Bacterial System for the Assembly of Iron-Sulfur Clusters with Homologs in Archaea and Plastids, J. Biol. Chem. 277 (2002) 28380–28383.
[57] J. Yu, I.R. Vassiliev, Y.S. Jung, J.H. Golbeck, L. McIntosh, Strains of *Synechocystis* sp. PCC 6803 with altered PsaC. I. Mutations incorporated in the cysteine ligands of the two [4Fe-4S] clusters FA and FB of photosystem I, J. Biol. Chem. 272 (1997) 8032–8039.
[58] J. Giner-Lamia, L. López-Maury, F.J. Florencio, Global transcriptional profiles of the copper responses in the cyanobacterium *Synechocystis* sp. PCC 6803, PLoS One 9 (2014), e108912.
[59] B. Voss, J. Georg, V. Schön, S. Ude, W.R. Hess, Biocomputational prediction of noncoding RNAs in model cyanobacteria, BMC Genomics 10 (2009) 123.

[60] M. Kopf, S. Klähn, I. Scholz, J.K.F. Matthiessen, W.R. Hess, B. Voß, Comparative Analysis of the Primary Transcriptome of *Synechocystis* sp. PCC 6803, DNA Res. 21 (2014) 527–539.
[61] Y. Shimoni, G. Friedlander, G. Hetzroni, G. Niv, S. Altuvia, O. Biham, H. Margalit, Regulation of gene expression by small non-coding RNAs: a quantitative view, Mol. Syst. Biol. 3 (2007) 138.
[62] P. Mandin, S. Chareyre, F. Barras, A Regulatory Circuit Composed of a Transcription Factor, IscR, and a Regulatory RNA, RyhB, Controls Fe-S Cluster Delivery, MBio 7 (2016).
[63] C.J. Schwartz, J.L. Giel, T. Patschkowski, C. Luther, F.J. Ruzicka, H. Beinert, P.J. Kiley, IscR, an Fe-S cluster-containing transcription factor, represses expression of Escherichia coli genes encoding Fe-S cluster assembly proteins, Proc. Natl. Acad. Sci. U. S. A. 98 (2001) 14895–14900.
[64] E. Massé, C.K. Vanderpool, S. Gottesman, Effect of RyhB small RNA on global iron use in *Escherichia coli*, J. Bacteriol. 187 (2005) 6962–6971.
[65] A. Tiwari, F. Mamedov, M. Grieco, M. Suorsa, A. Jajoo, S. Styring, M. Tikkanen, E.M. Aro, Photodamage of iron-sulphur clusters in photosystem I induces non-photochemical energy dissipation, Nat. Plants 2 (2016) 16035.
[66] P.S. Novichkov, A.E. Kazakov, D.A. Ravcheev, S.A. Leyn, G.Y. Kovaleva, R.A. Sutormin, M.D. Kazanov, W. Riehl, A.P. Arkin, I. Dubchak, et al., RegPrecise 3.0 – A resource for genome-scale exploration of transcriptional regulation in bacteria, BMC Genomics 14 (2013) 745.
[67] O. Schmitz, J. Gurke, H. Bothe, Molecular evidence for the aerobic expression of nifJ, encoding pyruvate:ferredoxin oxidoreductase, in cyanobacteria, FEMS Microbiol. Lett. 195 (2001) 97–102.